

Improving Identity-Robustness for Face Models

Qi Qi*

The University of Iowa
Iowa City, IA
qi-qi@uiowa.edu

Sherwin Ardeshir

Netflix
Los Gatos, CA
shervina@netflix.com

Abstract

Despite the success of deep-learning models in many tasks, there have been concerns about such models learning shortcuts, and their lack of robustness to irrelevant confounders. When it comes to models directly trained on human faces, a sensitive confounder is that of human identities. Many face-related tasks should ideally be identity-independent, and perform uniformly across different individuals (i.e. be fair). One way to measure and enforce such robustness and performance uniformity is through enforcing it during training, assuming identity-related information is available at scale. However, due to privacy concerns and also the cost of collecting such information, this is often not the case, and most face datasets simply contain input images and their corresponding task-related labels. Thus, improving identity-related robustness without the need for such annotations is of great importance. Here, we explore using off-the-shelf face-recognition embedding vectors, as proxies for identities, to enforce such robustness. We propose to use the structure in the face-recognition embedding space, to implicitly emphasize rare samples within each class. We do so by weighting samples according to their conditional inverse density (CID) in the proxy embedding space. Our experiments suggest that such a simple sample weighting scheme, not only improves the training robustness, it often improves the overall performance as a result of such robustness. We also show that employing such constraints during training results in models that are significantly less sensitive to different levels of bias in the dataset.

1. Introduction

Given the success of machine learning models, and their deployment at scale, having a more extensive evaluation of the robustness of such models is of utmost importance. Given the nature of training such models, there is always

the potential for these models to rely on irrelevant and spurious shortcuts. Relying on such shortcuts could have immense negative consequences when the dataset and tasks are defined around humans. A prevalent type of such datasets and tasks are those defined on human faces, ranging from regression tasks such as estimating pose[2], facial-landmarks[34], etc, to classification tasks such as facial-expressions classification[18], and generative tasks such as avatar creation[3], etc. A common attribute of many of such face-centric tasks is the fact that the model performance, should be identity independent by definition, yet this aspect of a model is often not taken into account during training and evaluation. Two models trained on a face-related task can have similar overall performance, but very different levels of robustness across different individuals. The toy example in Figure 1 illustrates this concept. This disparity in performance often gets baked into the model due to bias in the training data, as data points belonging to different sub-populations may have a different level of class imbalance. More specifically, if person 1 smiles 90% of the time, and person 2 smiles 10% of the time, a smile classifier can easily latch on to the facial features of person 1 as a shortcut to reduce training loss significantly. Thus, it could always label images of person-1 as smiling, because of the person's identity, and not the facial expression.

Awareness of identity/group labels would allow for mitigation approaches to prevent such bias, such as recent efforts in adversarial training [36, 14], model interpretation method [29] and objective regularization [6], which aim to reduce the disparity between different groups using the ground-truth group labels $g \in G$. In many practical scenarios, however, such information is not available at scale during training and evaluation. Also, collecting such detailed annotation could be costly and undesirable due to three main reasons: First, annotating every sample data point with all their potential types of group-membership information could be extremely costly. Second, collecting and maintaining such detailed categorical labels on human faces raise data-privacy concerns. And third, the nature of many types of such group memberships may be extremely

*Most of the work was done while the author was an intern at Netflix. The first version of the paper was released at April 7th, 2023.

subjective. In addition to the previous hurdles in obtaining such data, most current large-scale datasets, lack such annotations at scale, which is another testament to the need for approaches that are not reliant on the availability of such additional information. As a result, improving fairness when the ground-truth group labels $g \in G$ are unknown is of utmost importance, and has given rise to an area of research often referred to as "fairness under unawareness". When it comes to "fairness under unawareness" for face models, the only earlier work is [4] which aims to measure the performance disparity of a model in the absence of group information. A disparity method (Disparity across Embedding Neighborhoods) is proposed, which approximates Rawlsian Max-Min (RMM) across groups $g \in G$, solely based on face-recognition embedding vectors. The neighbors of a sample are defined as the samples whose euclidean distance in the face-recognition embedding space is less than a pre-defined threshold. The aforementioned work solely focused on approximating disparity for a given model. In this work, however, we focus on using such intuition to reduce such disparity during training and directly optimize for such an objective. In other words, given a face dataset and solely its task labels, and without any group information, we explore if we can use embeddings from an off-the-shelf face recognition model to reduce the performance disparity of such a model across different individuals.

As identity bias is often induced due to class imbalance within a subpopulation of a dataset, we propose to exploit the structure of the training data points in the face-recognition embedding space and enforce class balance for any subpopulation that shares similar facial features. This is achieved by weighting the samples according to their conditional inverse density (CID) in the proxy embedding space, resulting in equalizing the effect of task-positive and task-negative labels for each local neighborhood in the proxy embedding space. In other words, we aim to equalize the total weight for positive and negative samples for people whose facial features look like any arbitrary embedding z . Our experiments show that such a simple sample weighting scheme not only reduces the performance disparity of the trained model across different individuals and groups but also makes the training more robust to distribution shifts between train and test, and different levels of dataset bias. We evaluate such robustness by designing a stress test where we artificially manipulate the bias in the dataset, and control its level of bias.

2. Related Work

The bias mitigation methods can be broadly categorized into two groups based on the availability of group information, denoted by G . When G is available, the proposed methods usually explicitly incorporate such group information into the training process to reduce bias, such as penal-

izing the group difference as a regularizer [6, 8], enhancing fair representations via contrastive learning only using task-relevant features by constructing hard negative pairs from different groups [37, 26, 13], learning an adversary head to reduce models' ability to distinguish group-relevant features that amplify biases [36, 31], and so on.

Our work can be categorized under the "fairness under unawareness" umbrella, where group information G is unavailable during training. Due to the lack of group information, improving model robustness to minimize spurious correlations has become one of the mainstream methods to enhance model fairness. This can be achieved through various methods such as invariant risk minimization [5, 1], distributionally robust optimization [7, 10, 30, 15, 23, 27, 21], and class balancing methods [35, 11, 17, 33].

Invariant Risk Minimization (IRM) IRM [5] was proposed to address the domain-shifting problems by learning invariant feature representations that have good generalization ability between training and testing. To achieve this, IRM optimizes the losses across different data distributions to improve model robustness. [1] shows the effectiveness of IRM in reducing the disparity between different protected groups in the toxicity classification task on Civil Comments natural language process dataset when G is unavailable.

Distributionally Robust Optimization (DRO) Compared with ERM which minimizes the average sample losses, DRO aims to focus on the largest errors [7, 10] by assigning robust weights p_i to samples proportional to the loss scales. To verify the validity of DRO in improving fairness under unawareness, [24] empirically shows that most of the samples with the largest errors belong to the worst group, [15] theoretically proves that DRO can control group disparity amplification in every iteration, and [23, 27] shows the effectiveness of DRO in different fair applications. Recently, [21] proposed a generalized DRO method, namely Adversarially Reweighted Learning (ARL), by parameterizing the robust weight p_i with an adversarial network ϕ and leveraging the concept of a computationally-identifiable subgroup of largest errors [16] to improve model fairness.

Class Balancing [35] proposed a cluster-based balancing method by generating the minority samples for each cluster using the upsampling K-Means SMOTE [22], however, this upsampling clustering-based method only applicable to small tabular data and lead to excessive training time for larger datasets. Alternatively, class balancing reweighting methods [11, 17, 33] are widely used to improve model robustness in large datasets by assigning weights to balance the contribution of different classes. These weights of each sample are typically inversely proportional to the number of class samples, which helps to improve the performance of minority classes and alleviates the spurious correlations between the sensitive groups and classes incurred due to the lack of samples in minority class.

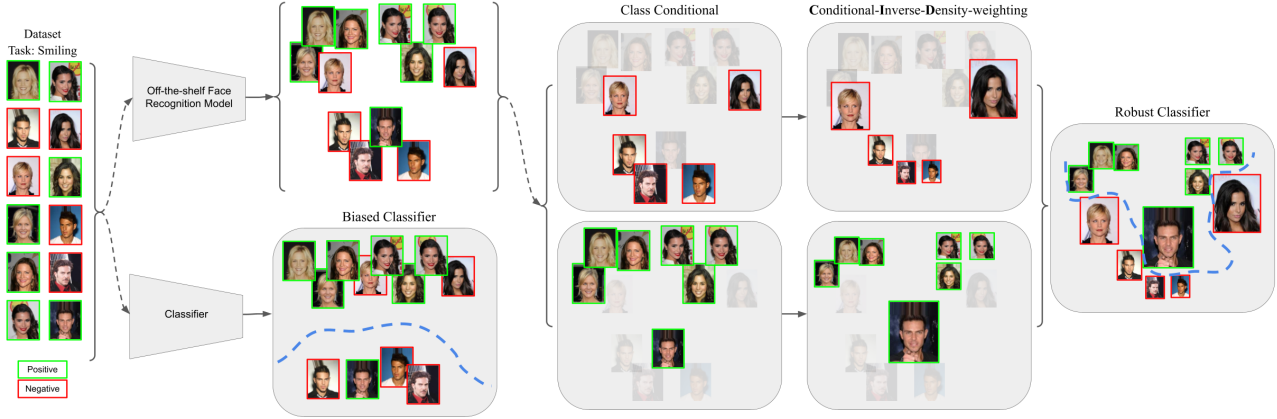


Figure 1. Toy example visualizing our proposed approach. The task is predicting if a face image is smiling (green) or not (red). The Biased Classifier shows how a biased dataset could lead to a model latching on to spurious features (identity) for an identity-independent task (smiling). We propose extracting face-recognition embeddings and using the structure in that space to weight rare samples within each class. More specifically, for each class (green or red), each sample is weighted based on its class-conditioned inverse density in the proxy (face recognition) embedding space. As a result, in each class, the rare samples are emphasized in the Robust Classifier.

To summarize, the IRM, DRO, and class-balancing methods rely on the implicit preservation of sensitive group (categorical) information in model predictions, either through losses [1, 7, 10, 30, 15, 23, 27] or feature representation embeddings [21, 35]. However, in our case, this assumption does not hold as we are focusing on face-centric tasks that are defined identity independent. Therefore, our CID method resorts to face recognition embeddings to have better group proxies. In the supplementary, we provide comparisons and draw parallels between our approach and the aforementioned methods under certain assumptions.

3. Approach

Given a dataset of images of faces, and an identity-independent face-related task such as predicting a facial expression (e.g. smiling), we aim to train a classifier that performs robustly across face images of different people. We refer to training labels related to the task of interest (smiling), as *task labels*. We assume that such labeling (whether a face is smiling or not) is given to us for training and test set. On the contrary, we assume that no *identity* label is given to us during training. Identity labels specify which images belong to which person (person-1, person-2, ...), across which we would like to enforce fairness/robustness. We also assume that we have access to an off-the-shelf face-recognition model, using which we can extract an embedding for each face image. Our goal is to train a model for that task, that performs robustly (fairly) across different individuals on the test set. Please note that in our experiments, we solely use the identity-labeled test sets to validate the robustness of our approach, and we do not use such labels during training. Formally, given a dataset $\mathcal{D} = \{X \times Y\} = \{(\mathbf{x}_i, y_i)\}_{i=1}^{|\mathcal{D}|}$ with size $n = |\mathcal{D}|$, the total number of classes

C , i.e. $|Y| = C$. $\mathcal{D}_y = \{(\mathbf{x}_i, y_i) | y_i = y, i \in [1, \dots, |\mathcal{D}|]\}$ represents the samples whose task label is $y \in Y$. $g_i \in G$ denotes the identity/group that sample i belongs to, across which performance disparity should be mitigated. Under our setup, group/identity labels G are unavailable during training. Instead, the embedding vectors $\{\mathbf{z}_i\}_{i=1}^{|\mathcal{D}|}$ are extracted from a face recognition model and are provided as proxies for the group/identity membership.

4. Training

Inspired by recent efforts in [12, 15, 21], we define our objective as a min-max form, which encourages emphasis the performance of the model on the least accurate areas of the embedding space:

$$\min_{\mathbf{w}} \sum_{i=1}^n \frac{p_i^\top}{Z_{y_i}} \ell(\mathbf{w}; \mathbf{x}_i, y_i) \quad (1)$$

$$\text{s.t. arg max}_{\mathbf{p}_i \in \Delta_{\mathcal{D}_{y_i}}} \sum_{j \in \mathcal{D}_{y_i}} p_{ij} \mathbf{z}_i^\top \mathbf{z}_j - \tau \text{KL}(\mathbf{p}_i, \frac{\mathbf{1}}{|\mathcal{D}_{y_i}|}) \quad (2)$$

where $p_i^\top := p_{ii}$ denotes the sample weight, $\ell(\mathbf{w}; \mathbf{x}_i, y_i)$ denotes the prediction loss, and $Z_{y_i} = \sum_{i \in \mathcal{D}_{y_i}} p_i^\top$ is the class-level normalization parameter to guarantee each class contributes equally. To obtain p_i^\top , the maximum constraint in (2) is imposed on the pairwise similarity of proxy embedding vectors, leveraging the proxy neighborhood structure associated with each sample. To be more specific, for $\forall (\mathbf{x}_i, y_i) \sim \mathcal{D}$, $\mathbf{p}_i = (p_{i1}, \dots, p_{ii}, \dots, p_{i|\mathcal{D}_{y_i}|})$ refers to the weight assigned to each sample based on $\{\mathbf{z}_i^\top \mathbf{z}_j\}_{j \in \mathcal{D}_{y_i}}$ and satisfies $\Delta_{\mathcal{D}_{y_i}} := \{\sum_j p_{ij} = 1, p_{ij} \geq 0\}$. The KL divergence regularizer $\sum_j p_{ij} \log(|\mathcal{D}_{y_i}| p_{ij})$ between the uniform distribution $1/|\mathcal{D}_{y_i}|$ and the pairwise weights \mathbf{p}_i encourages the model to focus on the local neighborhood. The

regularizer hyperparameter τ measures the proximity and magnitude of the neighborhood, which will be explained in next section.

4.1. Batch-wise Implementation using Conditional Inverse Density (CID)

Here we explain how we practically optimize the objective mentioned above using a sample-weighting scheme based on the conditional inverse density (CID for short) of each datapoint in the proxy embedding space. To expand, we consider the practical batch-wise training scheme such that the constraint set \mathcal{D}_{y_i} in Eqn (2) is defined as the samples having the same task labels in the current batch \mathcal{B} , i.e., \mathcal{B}_{y_i} (thus, conditioned on task label). Thanks to the strong concavity of \mathbf{p}_i in (2) and the specific structure of KL divergence, the close form solution of $p_i^\tau := p_{ii}$ is obtained by taking the first derivative of \mathbf{p} in (2) equals to 0, i.e.,

$$p_i^\tau = \frac{\exp(\frac{\mathbf{z}_i^\top \mathbf{z}_i}{\tau})}{|\mathcal{B}_{y_i}| \sum_{k=1}^{\mathcal{B}_{y_i}} \exp(\frac{\mathbf{z}_i^\top \mathbf{z}_k}{\tau})} \quad (3)$$

where the numerator is the exponential of the inner product of the proxy embedding vector \mathbf{z}_i of sample (\mathbf{x}_i, y_i) . The denominator explores the neighborhood proxy structure by aggregating of the exponential pairwise similarities of proxy vectors between sample (\mathbf{x}_i, y_i) and \mathcal{B}_{y_i} . Even though the constraint set is defined in \mathcal{B}_{y_i} , the skewness property of exponential function $\exp(\cdot/\tau)$ for large similarities pairs encourages the denominator to focus on the local neighbors of (\mathbf{x}_i, y_i) that share the same facial features. $p_i^\tau \in (0, 1]$ represents the importance of the sample (\mathbf{x}_i, y_i) in the local neighborhood. The fewer the samples in the local neighborhood, the higher the p_i^τ . Hence, p_i^τ is inverse proportional to the class-conditional sample density in the local neighborhood and emphasizes on the rare samples within each class.

In [4], the performance of a model across different local neighborhoods in the proxy embedding space is used to estimate disparity across identities/groups. Hence a local neighborhood could be seen as an approximation for a sub-population/group/identity g_i . [4] also illustrates that there are different neighborhood sizes that better approximate different group memberships. To capture the same concept, in our formulation τ controls the skewness of the exponential function, which influences the size of the local neighborhood. Thus, we fine-tune the hyper-parameter τ to allow for exploring different neighborhood sizes and therefore different density estimations. Figure 2 shows the impact of τ on the weight of three different samples. As it can be seen, as $\tau \rightarrow \infty$, the weights converge to $p_i^\tau \rightarrow \frac{1}{|\mathcal{B}_{y_i}|}$ which is simply the inverse of per-class frequency.

In the example shown in Figure 2, the blue and red circles come from the majority circle class, and the green trian-

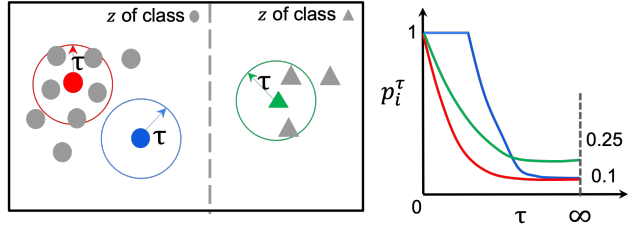


Figure 2. Visualizing the effect of τ on p_i^τ and the soft local neighborhood in the proxy vector space $\{\mathbf{z}\}_{i=1}^{|\mathcal{B}|}$ and $\mathbf{z} \in \mathbb{R}^2$. We plot the p_i^τ curves calculated according to equation (3) by varying τ for the red and blue dots from the circle class, and the green sample from the triangle class. The circle class and triangle class include 10 samples and 4 samples, respectively.

gle comes from the minority class. Often in typical sample weighting schemes, all samples within the same class are weighted uniformly and based on the inverse of their frequency. Thus samples in the minority class are always up-weighted compared to samples in the majority class. However, our sample weighting scheme allows for a more nuanced weighting. Compared with the blue circle, it can be observed that the red circle lies in the denser area, i.e. has more close neighbors. Hence, the p_i^τ of the red circle is consistently smaller than p_i^τ of the blue circle for the same $\tau \in (0, \infty)$. Also, they both converge to the inverse frequency $1/10$ when $\tau \rightarrow \infty$. When comparing samples from different classes, the green triangle (which is from the minority class) has more neighbors for smaller τ , and thus could have a smaller weight compared to the blue circle which comes from the majority class. This allows for capturing a more nuanced notion of sample rarity within each class, which goes beyond the typical frequency-based methods.

Given p_i^τ , the proposed CID method simply minimizing the objective (1) such that p_i^τ is normalized using Z_{y_i} to equalize the total contribution of each class. Algorithm 1 describes the practical implementation of the proposed CID method in minimizing the objective (1).

5. Evaluation

In addition to using standard classification accuracy metrics, we measure the robustness of the trained models using the following metrics.

5.1. Area Under DEN Curves (AUD)

[4] introduces a metric for estimating structural performance disparity across an embedding space, referred to as *Disparity across Embedding Neighborhoods* (DEN for short). The aforementioned study shows that such a metric is a good estimate of the performance disparity across groups when group information is not available. In fact, our objective function is specifically designed to minimize

Algorithm 1 CID Optimization (τ)

- 1: Model initialization \mathbf{w}_1 , proxy embeddings $\{\mathbf{z}_i\}_{i=1}^n$
 - 2: **for** $t = 1, \dots, T$ **do**
 - 3: Sample a batch of B samples $\mathcal{B} = \{(\mathbf{x}_i, y_i)\}_i^B \sim \mathcal{D}$
 - 4: Retrieve the proxy embedding vectors of batch samples, $\{\mathbf{z}_i\}_{i=1}^B$.
 - 5: Calculate p_i^τ according to Eqn (3) for $\forall (\mathbf{x}_i, y_i) \in \mathcal{B}$
 - 6: Calculate $Z_{y_i} = \sum_{j \in \mathcal{B}_{y_i}} p_j^\tau$
 - 7: Calculate CID loss: $\sum_{i \in \mathcal{B}} p_i^\tau \ell_i(\mathbf{w}_t) / (Z_{y_i})$
 - 8: Update \mathbf{w}_t using stochastic algorithms.
 - 9: **end for**
 - 10: **Return** \mathbf{w}_{T+1} .
-

such disparity, thus we evaluate this metric on the test set to validate our assumption.

5.2. Area Under Min-Max Curves (AUMM)

As mentioned earlier, we do not have access to group labels during training, however, to measure if our model is in fact more robust across groups, we use group labels in the test set to validate our hypothesis. In our setup, we mostly focus on robustness/fairness across individuals, and given that the number of individuals in a face dataset could be very large, we define a modification to the widely used Rawlsian min-max metric. In the Rawlsian min max metric [28], the ratio of the performance of the model is measured between the most and least accurate groups, i.e. $1 - \frac{\min_g(e_g)}{\max_g(e_g)} |_{g \in G}$. This measure is often very useful when the number of groups is very limited. However, given that in our instance, we are interested in measuring disparity across different people, the number of different individuals in the dataset could be very large. Therefore, using the ratio of performance only on the highest and lowest individual will ignore large portions of the dataset. Thus we modify the Rawlsian min-max formulation to measure the ratio of the bottom- $k\%$ and top- $k\%$ of groups instead.

$$\text{MM} = \left\{ 1 - \frac{\bar{e}_g^k}{\underline{e}_g^k} \right\}_{k=1}^{|G|} \quad (4)$$

where $k \in [1, \dots, |G|]$ denotes the index of groups. \bar{e}_g^k and \underline{e}_g^k are the average of top and bottom k group performance, respectively. Sweeping k , results in a curve, which we refer to as the Min Max Curve. We use the area under this curve, AUMM for short, as a metric for robustness across groups. The lower the AUMM, the more robust/fair the model is.

6. Experiments

We evaluate the proposed approach alongside a few other baselines, on several datasets in terms of overall performance and robustness. In section 6.1 we go over the datasets and tasks used in our evaluation. In section 6.3 we provide details on our evaluation protocol and provide

experimental results. Finally, in section 6.4 we propose and report a stress test to measure robustness to controlled bias. In all experiments, for each face-image in the datasets, we extract its face-recognition embedding vector \mathbf{z} using the face recognition model [19] and use it as its identity proxy.

6.1. Datasets and Setup

We selected datasets that contained identity-independent tasks, and also contained information about the identity of the faces in the test set, in order to be able to evaluate the robustness of the trained models across identities at test time. As mentioned earlier, we do not use any identity information during the training phase, and solely rely on off-the-shelf face-recognition embeddings [19] on the train set. In the following, we provide information on the three datasets used for experiments:

CelebA [25] has 200K face images and includes 10117 identities in total. Each image is labeled with 40 attributes/tasks. We pick two identity-independent tasks [25] $\{\textit{Smiling}, \textit{Mouse Slightly Open(MSO)}\}$ and train standard binary classification models to predict those tests. We train ResNet18 model for 20 epochs both on SGD optimizers [9]. The learning rate is tuned in $\{0.003, 0.005, 0.01\}$ for all the baselines. The hyperparameter τ in the CID method is tuned in $\{0.1 : 0.1 : 0.5\}$.

ExpW [38] (cleaned version) is a facial expression dataset that includes 85K images with 1002 identities (split into 80% train, 10% val, and 10% test), and 7 labels of facial expressions $\{\textit{angry}, \textit{disgust}, \textit{fear}, \textit{happy}, \textit{sad}, \textit{surprise}, \textit{neutral}\}$. To balance the size of the data scale and model capacity, we combine *sad-surprise-fear-neutral* as the new *ssfn* attribute to have enough positive samples ($\sim 19\%$) to learn a valid CNN model. Then we predict $\{\textit{angry}, \textit{disgust}, \textit{happy}, \textit{ssfn}\}$ expressions, respectively. Following the experimental setup in [32], we adopt the SGD optimizer to optimize all a 4-layers CNN model. The structure of the model is provided in the appendix. We train 40 epochs using SGD optimizer. The learning rate is tuned $\{0.1, 0.05, 0.01\}$ and decayed at the 20th epoch by a factor of 100. τ is tuned in $\{0.1 : 0.1 : 0.5\}$.

PugFig [20]¹ including 9K images with 111 identities (split into 80% train, 10% val, and 10% test). Each image is tagged with the binary labels of lighting position, $\{\textit{frontal}, \textit{non-frontal}\}$ and facial expression, $\{\textit{neutral}, \textit{non-neutral}\}$. We train models to predict each task separately. Due to the limited data scale, we train the PugFig on the pre-trained ResNet18 model and fine-tune the fully connected layer for 60 epochs using SGD optimizer. The batch size is 16 and the weight-decay parameter is $5e-4$. The learning rate is tuned in $\{0.005 : 0.001 : 0.01\}$ and decayed at the 30th epoch by a factor of 10. τ is tuned in $\{0.1 : 0.1 : 0.5\}$.

¹54K images of downloading URLs have been provided for the original dataset. But, most of them failed.

6.2. Baselines

We compare proposed approach (CID) with the following effective baselines on fairness under awareness setup:

IFW (inverse frequency weighting) [17, 33]: This is the typical sample weighting used to enforce class balance. Given N_p, N_n number of positive and negative samples, the weights for the positive class and negative class samples are set proportional to $1/N_p$ and $1/N_n$, respectively.

DRO (Distributionally Robust Optimization)[23, 27]: We implement the ABSGD [27] stochastic optimization method for optimizing $\max_{\mathbf{p}} \sum p_i \ell_i(\mathbf{w}) - \lambda \sum p_i \log np_i$. The hyperparameter λ for DRO is tuned in $\{0.1, 0.5, 1, 2, 5\}$

IRM (Invariant Risk Minimization): we optimize $\ell(\mathbf{w}) + \lambda \|\nabla_{v|v=1.0} \ell(v \cdot \mathbf{w})\|^2$ objective using the optimization framework of [5]. λ for IRM is tuned in $\{0.1 : 0.1 : 1\}$.

ARL (Adversarial Reweighted Learning)[21]: ARL optimizes $\min_{\mathbf{w}} \max_{\phi} p_i^{\phi} \ell_i(\mathbf{w})$, where $p_i^{\phi} = 1/n + f_i^{\phi} / \sum_i f_i^{\phi}$, where ϕ is a linear adversary model with output score f_i^{ϕ} ².

6.3. Measuring Robustness

We evaluate the performance of the baselines mentioned in Section 6.2, in terms of overall classification accuracy (Acc), average, and standard-deviation of per-identity accuracy (Id Acc and δ_{Id}). This is evaluated by measuring a model’s prediction accuracy for each identity (person) in the test set, and reporting mean and standard deviation. Ideally a high-performing and identity-robust model should maintain high Id Acc, while having low δ_{Id} . A low δ_{Id} is one of the metrics implying that the performance of the model is robust across identities and thus more fair. In addition, we report the accuracy on the least accurate 10% of identities in the test set. Plus, we evaluate the model in terms of area under DEN curve (referred to as AUD for short), proposed in [4], and explained in section 5.1, which measures the disparity of performance across different neighborhoods of the embedding space of the face-recognition embedding. The lower the AUD, the more robust the model is. Also, as described in section 5.2, we use the area under the min-max curve (AUMM for short) as another robustness metric. Given that this metric measures the disparity between the accuracy of the top-k and bottom-k identities, the lower the AUMM, the more identity-robust a model is.

Table 1, 2, and 3 report experimental results on CelebA, ExpW, and PubFig datasets respectively, and averaged over 5 independent runs. It can be observed that CID outperforms all the baselines in terms of every model robustness metric, namely, (lowest) 10% Id Acc, δ_{Id} , AUMM, and AUD. In addition, the overall accuracy is also either higher than baseline, or very competitive. In other words, CID does maintain high accuracy while attaining robustness.

²The details of implementation are provided in the supplementary.

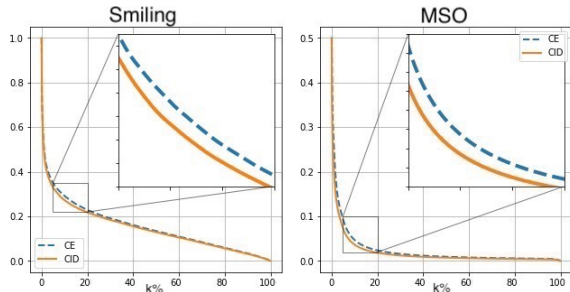


Figure 3. The Min-Max curves for the *Smiling* and *Mouth Slightly Open (MSO)* tasks. It can be observed that CID consistently yields a lower curve, resulting in a smaller area under the MM curve, and thus, less disparity across top and bottom k% identities.

Table 1. Attributes Prediction Experimental Results on CelebA. **Bold** and underline are best and second-best results of each metric.

Smiling	Acc	Id Acc	10% Id Acc	δ_{Id}	AUMM	AUD
CE	92.73	<u>92.02</u>	71.02	0.0962	<u>0.1544</u>	0.1156
IFW	92.69	92.99	71.03	0.0968	0.1550	<u>0.1141</u>
DRO	92.55	91.90	71.06	0.0965	0.1546	0.1146
IRM	92.71	92.11	<u>71.74</u>	0.0939	0.1522	0.1143
ARL	92.71	92.07	70.94	0.0975	0.1558	0.1151
CID	<u>92.72</u>	<u>92.15</u>	71.94	0.0926	0.1506	0.1126

MSO	Acc	Id Acc	10% Id Acc	δ_{Id}	AUMM	AUD
CE	94.09	93.71	74.57	0.0838	0.1322	0.1036
IFW	<u>94.09</u>	<u>93.73</u>	75.06	<u>0.0832</u>	<u>0.1305</u>	0.1019
DRO	94.04	93.69	75.07	0.0840	0.1341	0.1038
IRM	94.04	92.68	<u>75.10</u>	0.0837	0.1325	0.1021
ARL	93.97	93.54	74.04	0.0871	0.1376	0.1033
CID	94.13	93.79	75.36	0.0824	0.1299	0.1005

6.4. Stress-testing with Controlled Bias

In this section, we aim to measure how sensitive to dataset bias a model is by stress testing the model. To do so, we construct different versions of the train/validation sets of CelebA, by manipulating the dataset and adding controlled artificial identity-to-task bias. More specifically, given a task (such as smiling), we construct a biased train set by excluding $p\%$ of data points belonging to a (task-label, sub-population). As an example, in one of the variations, we exclude 50% of male-smiling images. This would artificially create a biased dataset that is prone to correlating male faces to the label non-smiling. If we train a classifier on such a dataset, a model’s performance on the standard (non-manipulated) test set can be very non-robust, as the train and test set do not follow the same distribution. In all the setups we solely manipulate the bias in the train set and keep the test set unchanged. We try this experiment for different values of $p \in \{25\%, 50\%, 75\%, 90\%\}$, and for different (group, task-label) combinations. We refer to each setting by specifying which group (M:Male vs. F:Female), and which task label (P: positive, N: negative) has been manipulated (excluded by $p\%$) from the training and validation set (while the test set is unchanged). As an example, on the task “Smiling”, FP 50% means that half of the Female Positives

Table 2. Expression Prediction Experimental Results on ExpW.

Angry	Acc	Id Acc	10% Id Acc	δ_{id}	AUMM	AUD
CE	<u>63.25</u>	<u>63.26</u>	<u>33.46</u>	0.1706	0.3603	0.2270
IFW	60.83	60.84	32.29	<u>0.1691</u>	0.3643	0.2309
DRO	63.18	63.19	33.26	0.1693	0.3622	<u>0.2205</u>
IRM	63.17	63.18	33.20	0.1712	0.3615	0.2232
ARL	63.44	63.45	33.43	0.1693	<u>0.3584</u>	0.2214
CID	63.53	63.53	33.53	0.1672	0.3543	0.2188
Disgust	Acc	Id Acc	10% Id Acc	δ_{id}	AUMM	AUD
CE	75.23	75.23	<u>46.19</u>	0.1517	<u>0.2862</u>	0.1875
IFW	74.93	74.94	44.99	<u>0.1514</u>	0.2938	<u>0.1758</u>
DRO	<u>75.26</u>	<u>75.27</u>	46.09	0.1520	0.2865	0.1867
IRM	75.25	75.27	46.00	0.1518	0.2863	0.1921
ARL	75.13	75.14	45.80	0.1531	0.2893	0.1911
CID	75.27	75.28	46.22	0.1503	0.2837	0.1749
Happy	Acc	Id Acc	10% Id Acc	δ_{id}	AUMM	AUD
CE	86.94	86.95	59.28	0.1292	0.2159	0.1429
IFW	86.86	86.87	59.24	0.1290	0.2160	0.1326
DRO	86.95	86.96	59.34	<u>0.1286</u>	0.2151	<u>0.1311</u>
IRM	<u>86.98</u>	<u>87.00</u>	<u>59.73</u>	0.1289	<u>0.2148</u>	0.1386
ARL	86.73	86.95	0.5957	0.1290	0.2166	0.1391
CID	87.00	87.01	59.99	0.1281	0.2140	0.1251
SSFN	Acc	Id Acc	10% Id Acc	δ_{id}	AUMM	AUD
CE	<u>85.16</u>	<u>85.17</u>	58.85	0.1273	<u>0.2187</u>	0.1583
IFW	79.98	79.99	53.13	0.1434	0.2588	0.1695
DRO	85.19	85.20	58.95	0.1278	0.2200	<u>0.1583</u>
IRM	85.20	85.21	<u>59.08</u>	<u>0.1271</u>	0.2197	0.1632
ARL	85.07	84.51	57.52	0.1342	0.2259	0.1655
CID	85.14	85.15	59.60	0.1260	0.2163	0.1576

Table 3. Experimental Results on PubFig.

Frontal	Acc	Id Acc	10% Id Acc	δ_{id}	AUMM	AUD
CE	74.83	74.93	36.11	<u>0.1913</u>	0.3487	<u>0.1639</u>
IFW	71.68	71.77	34.72	0.1969	0.3582	0.1837
DRO	74.60	74.70	37.15	0.1930	0.3491	0.1660
IRM	<u>75.13</u>	<u>75.24</u>	<u>37.85</u>	0.1974	<u>0.3465</u>	0.1657
ARL	73.56	74.77	37.85	0.1931	0.3479	0.1655
CID	75.10	75.20	38.19	0.1906	0.3449	0.1606
Neutral	Acc	Id Acc	10% Id Acc	δ_{id}	AUMM	AUD
CE	56.48	56.55	26.74	0.1798	<u>0.3985</u>	0.2645
IFW	<u>56.61</u>	56.69	26.74	<u>0.1773</u>	0.4050	0.2593
DRO	56.24	56.32	26.74	0.1782	0.4034	0.2588
IRM	56.48	56.55	<u>27.08</u>	0.1817	0.4009	<u>0.2582</u>
ARL	56.91	55.85	26.04	0.1772	0.3995	0.2575
CID	56.51	<u>56.59</u>	27.43	0.1677	0.3864	0.2544

(smiling female faces) were excluded during training, therefore creating a bias in the dataset. Combinations of these setups could also be generated to further exaggerate the bias (such as FPMN: removing positive/smiling female images and negative/non-smiling male images). Figure 4 shows the results of our stress test on the task "Smiling". Due to space limitations, we only report the robustness measures, namely, MMC, δ_{id} , AUMM, and bottom 10% Id Acc experimental results between CE (cross-entropy) and CID on all different setups and levels of induced bias. We also provide more stress test results, including other metrics, analysis on the other CelebA task, and other variations of the manipulation setups in the supplementary. All other variations of

tasks, metrics and setups follow the same trend.

Table 4. Stress testing the models on the CelebA dataset, by eliminating 90% of a subpopulation in the training/validation set.

FP	Acc	Id Acc	10% Id Acc	δ_{id}	AUMM	AUD
CE	90.33	89.77	65.91	0.1095	0.1821	0.1354
IFW	91.13	90.49	<u>67.28</u>	<u>0.1053</u>	<u>0.1737</u>	<u>0.1259</u>
DRO	90.23	89.84	66.20	0.1098	0.1834	0.1367
IRM	<u>91.18</u>	90.11	66.54	0.1088	0.1789	0.1343
ARL	90.40	89.46	65.55	0.1127	0.1863	0.1323
CID	91.31	90.67	67.73	0.1042	0.1717	0.1233
FN	Acc	Id Acc	10% Id Acc	δ_{id}	AUMM	AUD
CE	89.42	89.51	66.52	0.1077	0.1821	0.1476
IFW	<u>90.47</u>	<u>90.29</u>	<u>67.45</u>	<u>0.1074</u>	<u>0.1761</u>	<u>0.1281</u>
DRO	89.43	89.51	66.53	0.1077	0.1817	0.1501
IRM	90.18	89.91	66.84	0.1075	0.1799	0.1438
ARL	89.64	89.66	66.78	0.1075	0.1807	0.1456
CID	90.89	90.58	68.12	0.1057	0.1727	0.1241
MP	Acc	Id Acc	10% Id Acc	δ_{id}	AUMM	AUD
CE	<u>91.51</u>	90.03	64.50	0.1162	0.1885	0.1349
IFW	91.34	<u>90.35</u>	<u>65.69</u>	<u>0.1127</u>	<u>0.1820</u>	<u>0.1309</u>
DRO	91.12	90.13	64.70	0.1172	0.1855	0.1381
IRM	91.22	90.23	65.01	0.1168	0.1823	0.1361
ARL	91.27	90.17	64.49	0.1169	0.1890	0.1371
CID	91.58	90.62	66.68	0.1091	0.1774	0.1221
MN	Acc	Id Acc	10% Id Acc	δ_{id}	AUMM	AUD
CE	90.29	89.53	63.72	0.1151	0.1922	0.1433
IFW	90.07	<u>90.24</u>	<u>65.68</u>	<u>0.1093</u>	<u>0.1816</u>	<u>0.1372</u>
DRO	90.03	89.60	63.91	0.1146	0.1915	0.1490
IRM	90.06	89.70	64.11	0.1123	0.1845	0.1455
ARL	<u>90.33</u>	89.51	63.54	0.1162	0.1956	-
CID	91.20	90.43	66.16	0.1080	0.1783	0.1241
FPMN	Acc	Id Acc	10% Id Acc	δ_{id}	AUMM	AUD
CE	87.25	86.48	57.28	0.1295	0.2229	<u>0.1584</u>
IFW	87.23	86.41	57.66	0.1322	0.2279	0.1655
DRO	<u>87.37</u>	<u>86.62</u>	<u>59.14</u>	<u>0.1280</u>	<u>0.2208</u>	0.1625
IRM	87.36	86.63	59.13	0.1283	0.2210	0.1614
ARL	87.32	86.55	58.33	0.1303	0.2247	0.1631
CID	87.87	87.09	60.24	0.1264	0.2170	0.1553

Table 5. Accuracy of the model on the least accurate subpopulation in the CelebA dataset $\{task-label \times Male/Female\}$ on the stress testing CelebA dataset. It can be observed that CID achieves the highest worst-case accuracy, and therefore the most robust among the evaluated baselines.

	FP	FN	MP	MN	FPMN
CE	83.32	76.96	72.87	78.09	<u>76.24</u>
IFW	<u>87.87</u>	<u>80.24</u>	<u>75.46</u>	82.46	73.34
DRO	83.16	76.98	73.05	78.40	76.19
IRM	83.77	77.04	73.51	78.33	75.93
ARL	83.09	76.47	74.37	78.32	75.62
CID	88.26	82.95	77.51	83.88	76.47

We observe that training models on these biased versions would cause their test performance to reduce (degrade) as the amount of bias increases. Similarly, disparity metrics increase (degrade) with more bias, as expected. This shows that our stress-testing framework in fact does introduce controlled bias to the trained model. We make the following observations from these experiments: 1) For each $\{task-label$

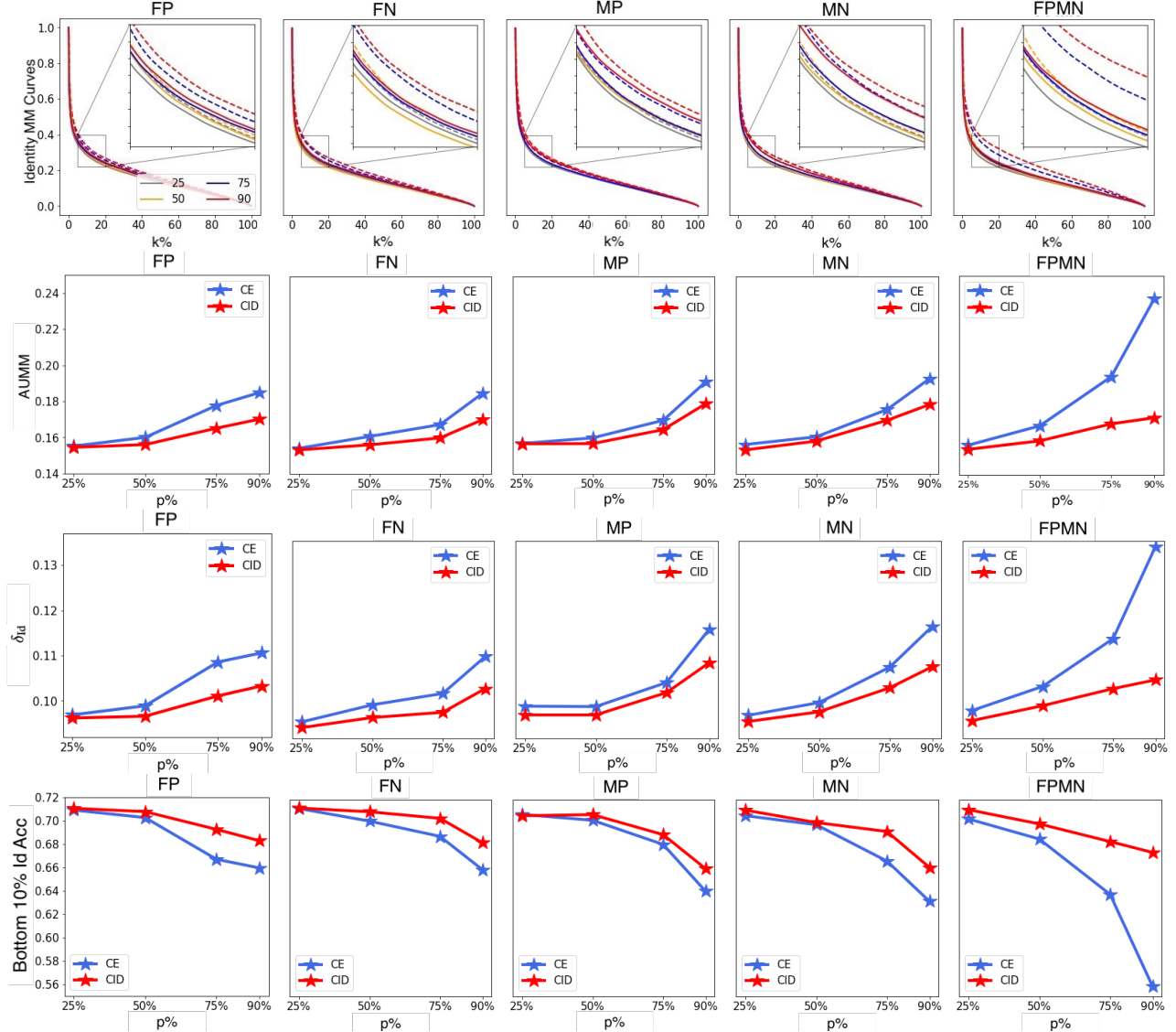


Figure 4. Results of different stress tests on the CelebA dataset for the smiling task label. The identity MM curves, area under identity min-max curves (AUMM), standard deviation of Id accuracy δ_{id} , and the bottom 10% percentage Id accuracy are measured for different setups and under different levels of induced bias. First row: For the MM figure, the x-axis shows k for which the disparity between top and bottom k identities is evaluated. In each figure, x-axis specifies the amount (percentage) of the training data of the (group, task-label) that is excluded during training. As it can be observed in all instances. As it can be observed, CID maintains its original metrics significantly better than CE in the presence of distribution shift.

× *Male/Female*} combination, the higher the amount of manipulation, the higher the MMC and AUMM values, which implies that the proposed metrics (MMC and AUMM) do capture the amount of bias in a model. 2) The proposed CID method has smaller MMC, AUMM, and δ_{id} values, in addition to higher bottom 10% Id accuracy compared to CE. The gap between the models steadily increases as the amount of induced bias in the dataset increases, which verifies the advantages of CID on handling distribution shifting over Empirical Risk Minimization. To narrow down

the scope, we report experimental results that compare CID with more baseline methods on the most biased version of each stress-test setup (i.e. MP 90%, MN 90%, FP 90%, FN 90%, and FPMN 90% in Table 4). Please note, given that we need access to group labels such as Male/Female and identity labels, we were only able to conduct this specific experiment on the CelebA dataset. To conclude this stress-test, all robustness metrics are significantly more desirable for CID compared to the baselines, alluding to the fact that our CID weighting scheme successfully mitigates bias, and

maintains high accuracy in presence of it. To make our experiments complement, we report the worst group accuracy that is widely used in the baseline comparison in terms of $\{task\text{-}label \times Male/Female\}$ in Table 5.

7. Conclusion

We propose a framework to effectively use off-the-shelf face-recognition model embeddings to improve the robustness/fairness of identity-independent face models. Our experiments show that our simple sample-weighting approach helps face models to maintain high accuracy while gaining significant robustness to distribution shifts and different levels of bias, and often maintaining a more uniform performance across different identities (and groups) of faces.

References

- [1] Robert Adragna, Elliot Creager, David Madras, and Richard Zemel. Fairness and robustness in invariant learning: A case study in toxicity classification. *arXiv preprint arXiv:2011.06485*, 2020. 2, 3
- [2] Vitor Albiero, Xingyu Chen, Xi Yin, Guan Pang, and Tal Hassner. img2pose: Face alignment and detection via 6dof, face pose estimation. In *Proceedings of the IEEE/CVF conference on computer vision and pattern recognition*, pages 7617–7627, 2021. 1
- [3] Thiemo Alldieck, Marcus Magnor, Weipeng Xu, Christian Theobalt, and Gerard Pons-Moll. Detailed human avatars from monocular video. In *2018 International Conference on 3D Vision (3DV)*, pages 98–109. IEEE, 2018. 1
- [4] Shervin Ardeshtir, Cristina Segalin, and Nathan Kallus. Estimating structural disparities for face models. In *Proceedings of the IEEE/CVF Conference on Computer Vision and Pattern Recognition*, pages 10358–10367, 2022. 2, 4, 6, 12
- [5] Martin Arjovsky, Léon Bottou, Ishaan Gulrajani, and David Lopez-Paz. Invariant risk minimization. *arXiv preprint arXiv:1907.02893*, 2019. 2, 6
- [6] Yahav Bechavod and Katrina Ligett. Penalizing unfairness in binary classification. *arXiv preprint arXiv:1707.00044*, 2017. 1, 2
- [7] Aharon Ben-Tal, Dick Den Hertog, Anja De Waegenare, Bertrand Melenberg, and Gijs Rennen. Robust solutions of optimization problems affected by uncertain probabilities. *Management Science*, 59(2):341–357, 2013. 2, 3
- [8] Alex Beutel, Jilin Chen, Tulsee Doshi, Hai Qian, Li Wei, Yi Wu, Lukasz Heldt, Zhe Zhao, Lichan Hong, Ed H Chi, et al. Fairness in recommendation ranking through pairwise comparisons. In *Proceedings of the 25th ACM SIGKDD international conference on knowledge discovery & data mining*, pages 2212–2220, 2019. 2
- [9] Léon Bottou. Stochastic gradient descent tricks. In *Neural networks: Tricks of the trade*, pages 421–436. Springer, 2012. 5
- [10] Simon Caton and Christian Haas. Fairness in machine learning: A survey. *arXiv preprint arXiv:2010.04053*, 2020. 2, 3
- [11] Yin Cui, Menglin Jia, Tsung-Yi Lin, Yang Song, and Serge Belongie. Class-balanced loss based on effective number of samples. In *Proceedings of the IEEE/CVF conference on computer vision and pattern recognition*, pages 9268–9277, 2019. 2
- [12] Emily Diana, Wesley Gill, Michael Kearns, Krishnaram Kenthapadi, and Aaron Roth. Minimax group fairness: Algorithms and experiments. In *Proceedings of the 2021 AAAI/ACM Conference on AI, Ethics, and Society*, pages 66–76, 2021. 3
- [13] Mengnan Du, Subhabrata Mukherjee, Guanchu Wang, Ruixiang Tang, Ahmed Awadallah, and Xia Hu. Fairness via representation neutralization. *Advances in Neural Information Processing Systems*, 34:12091–12103, 2021. 2
- [14] Yanai Elazar and Yoav Goldberg. Adversarial removal of demographic attributes from text data. *arXiv preprint arXiv:1808.06640*, 2018. 1

- [15] Tatsunori Hashimoto, Megha Srivastava, Hongseok Namkoong, and Percy Liang. Fairness without demographics in repeated loss minimization. In *International Conference on Machine Learning*, pages 1929–1938. PMLR, 2018. [2](#), [3](#)
- [16] Ursula Hébert-Johnson, Michael Kim, Omer Reingold, and Guy Rothblum. Multicalibration: Calibration for the (computationally-identifiable) masses. In *International Conference on Machine Learning*, pages 1939–1948. PMLR, 2018. [2](#)
- [17] Chen Huang, Yining Li, Chen Change Loy, and Xiaoou Tang. Learning deep representation for imbalanced classification. In *Proceedings of the IEEE conference on computer vision and pattern recognition*, pages 5375–5384, 2016. [2](#), [6](#), [15](#)
- [18] Yunxin Huang, Fei Chen, Shaohe Lv, and Xiaodong Wang. Facial expression recognition: A survey. *Symmetry*, 11(10):1189, 2019. [1](#)
- [19] Davis King. <https://github.com/davisking/dlib-models>. [5](#)
- [20] Neeraj Kumar, Alexander C Berg, Peter N Belhumeur, and Shree K Nayar. Attribute and simile classifiers for face verification. In *2009 IEEE 12th international conference on computer vision*, pages 365–372. IEEE, 2009. [5](#)
- [21] Preethi Lahoti, Alex Beutel, Jilin Chen, Kang Lee, Flavien Prost, Nithum Thain, Xuezhi Wang, and Ed Chi. Fairness without demographics through adversarially reweighted learning. *Advances in neural information processing systems*, 33:728–740, 2020. [2](#), [3](#), [6](#), [13](#)
- [22] F Last, G Douzas, and F Bacao. Oversampling for imbalanced learning based on k-means and smote. *arXiv preprint arXiv:1711.00837*, 2017. [2](#)
- [23] Tian Li, Ahmad Beirami, Maziar Sanjabi, and Virginia Smith. On tilted losses in machine learning: Theory and applications. *arXiv preprint arXiv:2109.06141*, 2021. [2](#), [3](#), [6](#), [14](#)
- [24] Evan Z Liu, Behzad Haghgoo, Annie S Chen, Aditi Raghunathan, Pang Wei Koh, Shiori Sagawa, Percy Liang, and Chelsea Finn. Just train twice: Improving group robustness without training group information. In *International Conference on Machine Learning*, pages 6781–6792. PMLR, 2021. [2](#)
- [25] Ziwei Liu, Ping Luo, Xiaogang Wang, and Xiaoou Tang. Deep learning face attributes in the wild. In *Proceedings of International Conference on Computer Vision (ICCV)*, December 2015. [5](#)
- [26] Sungho Park, Jewook Lee, Pilhyeon Lee, Sunhee Hwang, Dohyung Kim, and Hyeran Byun. Fair contrastive learning for facial attribute classification. In *Proceedings of the IEEE/CVF Conference on Computer Vision and Pattern Recognition*, pages 10389–10398, 2022. [2](#)
- [27] Qi Qi, Yi Xu, Rong Jin, Wotao Yin, and Tianbao Yang. Attentional biased stochastic gradient for imbalanced classification. *arXiv preprint arXiv:2012.06951*, 2020. [2](#), [3](#), [6](#), [14](#)
- [28] John Rawls. *Justice as fairness: A restatement*. Harvard University Press, 2001. [5](#)
- [29] Laura Rieger, Chandan Singh, William Murdoch, and Bin Yu. Interpretations are useful: penalizing explanations to align neural networks with prior knowledge. In *International conference on machine learning*, pages 8116–8126. PMLR, 2020. [1](#)
- [30] Shiori Sagawa, Pang Wei Koh, Tatsunori B Hashimoto, and Percy Liang. Distributionally robust neural networks for group shifts: On the importance of regularization for worst-case generalization. *arXiv preprint arXiv:1911.08731*, 2019. [2](#), [3](#)
- [31] Christina Wadsworth, Francesca Vera, and Chris Piech. Achieving fairness through adversarial learning: an application to recidivism prediction. *arXiv preprint arXiv:1807.00199*, 2018. [2](#)
- [32] Yisen Wang, Xingjun Ma, Zaiyi Chen, Yuan Luo, Jinfeng Yi, and James Bailey. Symmetric cross entropy for robust learning with noisy labels. In *Proceedings of the IEEE/CVF International Conference on Computer Vision*, pages 322–330, 2019. [5](#)
- [33] Yu-Xiong Wang, Deva Ramanan, and Martial Hebert. Learning to model the tail. *Advances in neural information processing systems*, 30, 2017. [2](#), [6](#), [15](#)
- [34] Yue Wu and Qiang Ji. Facial landmark detection: A literature survey. *International Journal of Computer Vision*, 127(2):115–142, 2019. [1](#)
- [35] Shen Yan, Hsien-te Kao, and Emilio Ferrara. Fair class balancing: Enhancing model fairness without observing sensitive attributes. In *Proceedings of the 29th ACM International Conference on Information & Knowledge Management*, pages 1715–1724, 2020. [2](#), [3](#)
- [36] Brian Hu Zhang, Blake Lemoine, and Margaret Mitchell. Mitigating unwanted biases with adversarial learning. In *Proceedings of the 2018 AAAI/ACM Conference on AI, Ethics, and Society*, pages 335–340, 2018. [1](#), [2](#)
- [37] Fengda Zhang, Kun Kuang, Long Chen, Yuxuan Liu, Chao Wu, and Jun Xiao. Fairness-aware contrastive learning with partially annotated sensitive attributes. In *The Eleventh International Conference on Learning Representations*. [2](#)
- [38] Zhanpeng Zhang, Ping Luo, Chen-Change Loy, and Xiaoou Tang. Learning social relation traits from face images. In *Proceedings of the IEEE International Conference on Computer Vision*, pages 3631–3639, 2015. [5](#)

8. Appendix

Due to space limitations, we omitted including some additional experimental results pertaining to stress tests, which we provide here in Section 8.1. We include an additional ablation study on the effect of the hyper-parameter τ , on our robustness metric AUMM, δ_{id} , and accuracy in Section 8.2. In Section 8.3, we report the Rawlsian min-max (RMM) results on identity-related gender and age groups for different methods. Finally, we describe the detailed implementation of ARL, and provide connections and comparisons between CID and baselines in Section 8.4.

8.1. More Results on the stress-tests

Here we provide additional results to complete the ones provided in Section 6.4. In Table 6 we provide results on the biased dataset under the FNMP (excluding 90% of female-negative and male-positive smiling examples) setup. Trends are similar to the experiments included in the main manuscript under Section 6.4. We also provide results on the other task of CelebA, namely, Mouth Slightly Open (MSO) in Figure 5. As mentioned in the main manuscript, all trends are similar to the smiling task, in terms of CID being consistently more accurate and less sensitive to bias, compared to CE. Also, the gap between the two models increases as bias in the dataset increases. In Table 7, we provide results on the biased CelebA dataset under FP 90%, MN 90%, and FPMN 90% setup. Trends are also consistently similar to the smiling tasks under section 6.4. In addition, we also add the trends in accuracy and ID-accuracy in the smiling task in Figure 6.

Table 6. Stress testing the models for the smiling task on the CelebA dataset, by eliminating 90% of the FNMP subpopulation (90% of the female-negative samples, and 90% of the male-positive samples) in the training/validation set. CID achieves the best results on the non-modified test set. This is consistent with other settings reported in Section 6.4.

FNMP	Acc	Id Acc	10% Id Acc	δ_{id}	AUMM	AUD
CE	87.61	87.28	60.47	0.1252	0.2137	0.1479
IFW	87.75	86.28	60.13	0.1256	0.2161	0.1533
DRO	87.85	<u>87.45</u>	<u>60.64</u>	<u>0.1240</u>	<u>0.2122</u>	0.1535
IRM	87.77	86.23	60.29	0.1256	0.2145	0.1493
ARL	<u>88.10</u>	86.82	59.33	0.1285	0.2194	0.1539
CID	88.44	87.93	61.54	0.1224	0.2068	0.1465

8.2. Ablation Studies on τ

In this section, we provide ablation studies of τ on the smiling task on CelebA, to show its effect on the results of the proposed CID method. As mentioned in the main manuscript in Section 4.1, and shown in Figure 2, this hyper-parameter implicitly captures the neighborhood radius across which performance is encouraged to remain uniform. In Figure 7, we report the AUMM, δ_{id} , and Accuracy by varying $\tau \in [0.01, 0.9]$ on the default dataset and

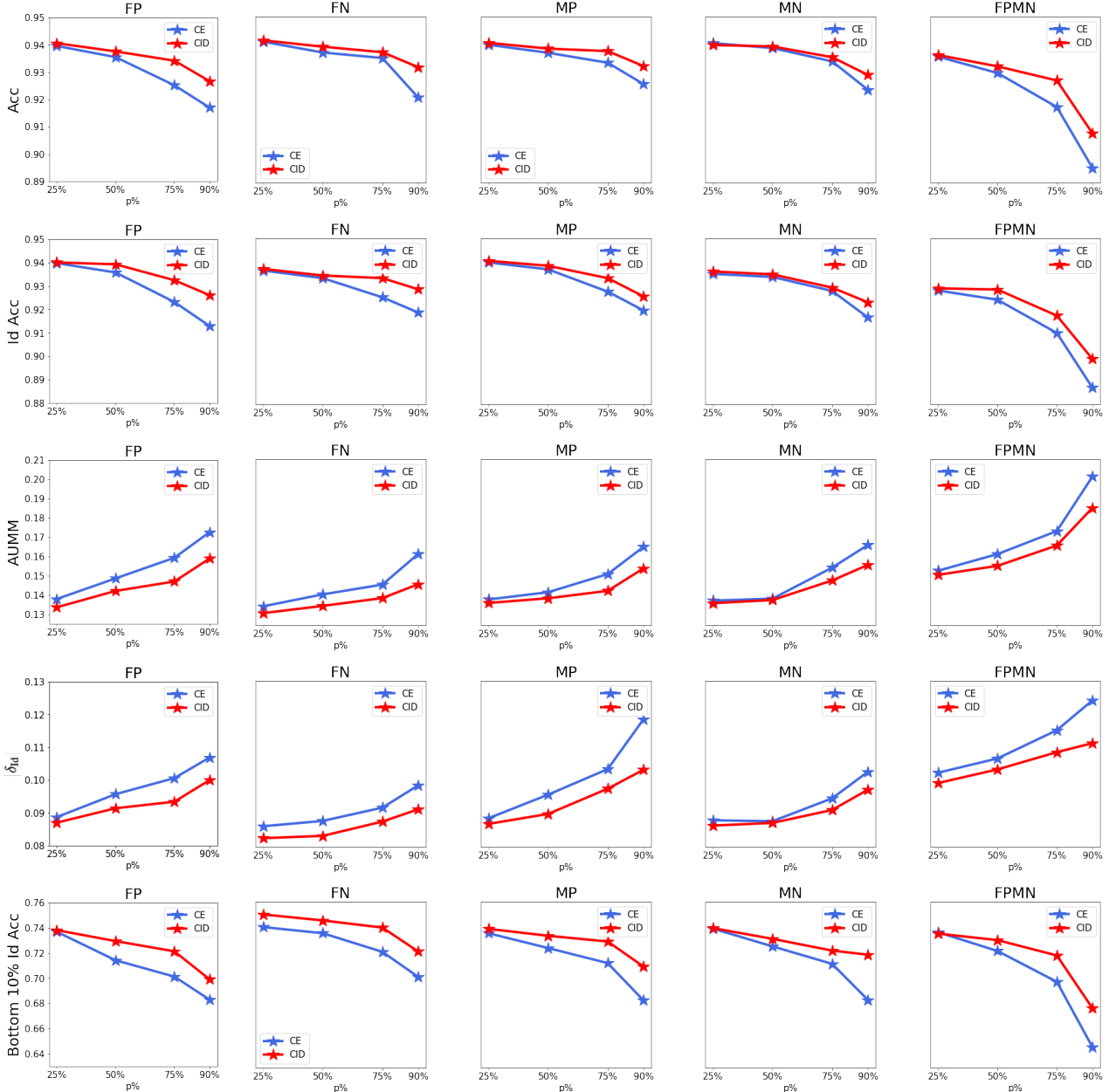


Figure 5. Results of different stress tests on the CelebA dataset for the mouth slightly open (MSO) task. We observe trends similar to the ones in the smiling task reported in Figure 4. CID seems consistently more robust, and less sensitive to bias compared to CE.

stressed FP 90%, MN 90%, FPMN 90% datasets. As it can be observed we can see the optimal value (lowest AUMM) is always achieved at 0.1. We hypothesize that as this maps to a specific radius in the embedding space, it captures the optimal neighborhood size for an individual person in the proxy embedding space. This is fairly consistent with the results reported in [4] regarding a specific radius being best for estimating individual fairness.

8.3. Rawlsian Min-Max (RMM) on gender and age

To complete our experiments, we report fairness in terms of identity-related gender and age attributes. Given that identity groups are defined by a unique set of characteristics, enhancing the fairness of identity can result in improved fairness across gender and age groups. As gender (*Male* or not) and age (*Young* or not) are labeled as binary in CelebA, we evaluate Rawlsian max-min (RMM) to measure disparity. We compare CID with other baselines and

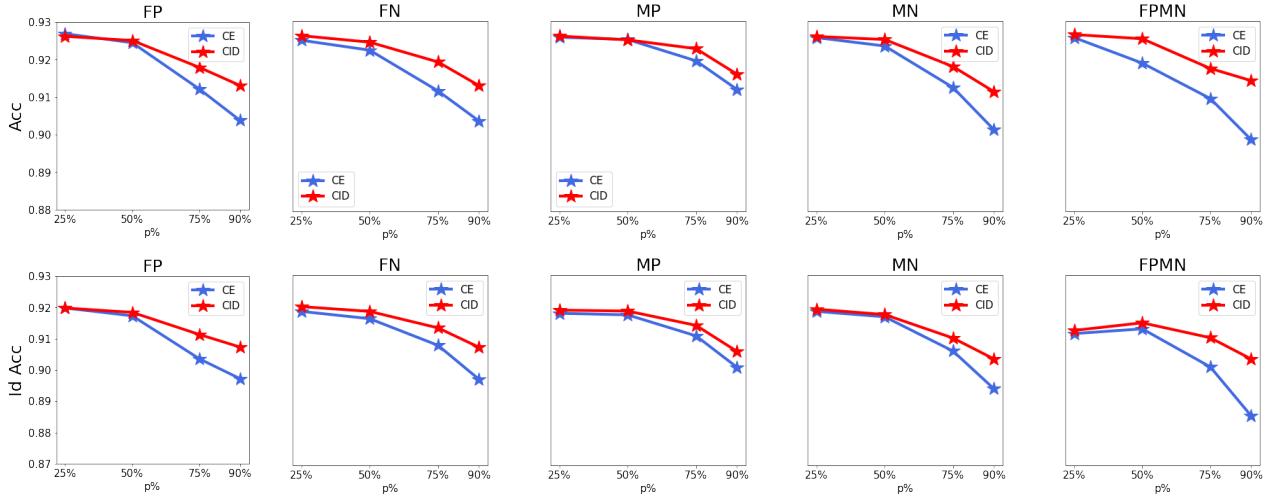


Figure 6. Accuracy (Acc) and average per-Id Accuracy (Id Acc) results of different stress tests on the CelebA dataset for the smiling task label. It can be observed that the trend is similar to other metrics in terms of CID being more robust to bias and maintaining higher overall accuracy.

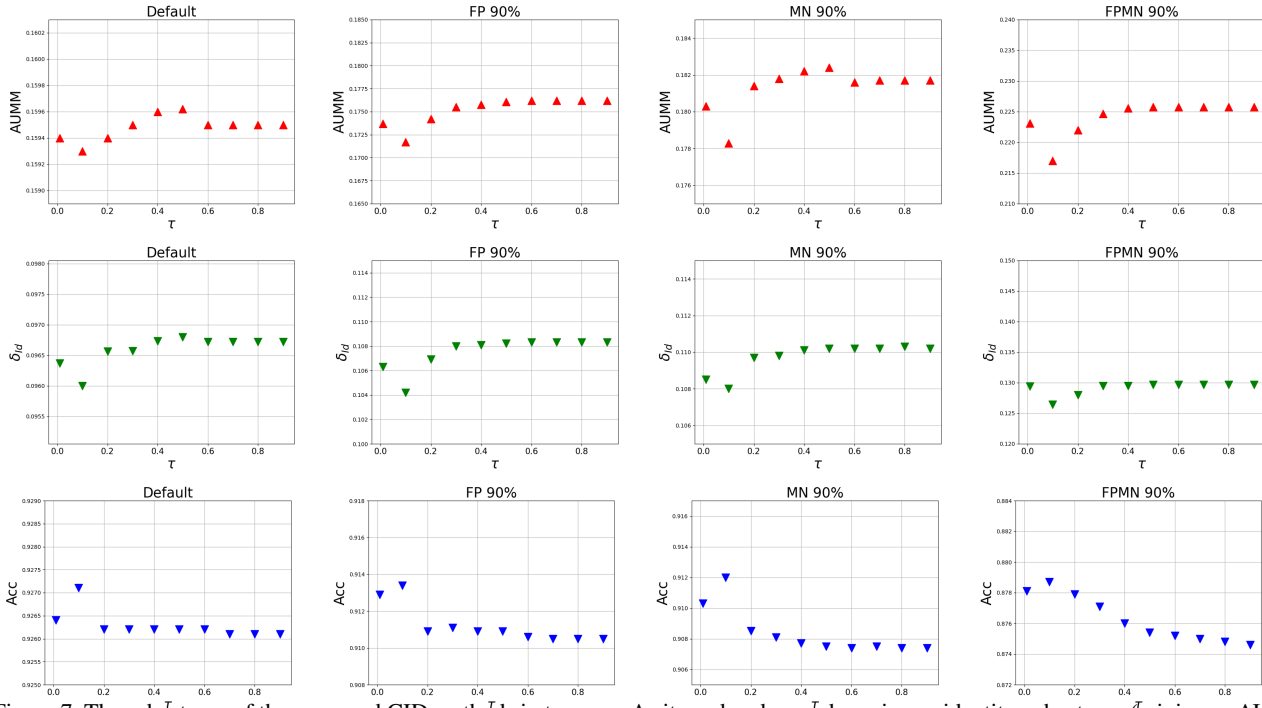


Figure 7. The robustness of the proposed CID methods in terms τ . As it can be observed maximum identity-robustness (minimum AUMM and δ_{id}), and maximum accuracy are achieved almost consistently at $\tau=0.1$

report the results in Table 8 under different setups on the Smiling task of CelebA, the improved (reduced) RMM verifies the effectiveness of the CID method on binary identity-related attributes.

8.4. Connects and Comparison with other baselines

In this section, we draw parallels and provide comparisons of CID with the methods that can be broadly cate-

gorized into the sample weighting scheme including ARL, DRO, and IFW class-balancing method.

8.4.1 Adversarially Reweighted Learning (ARL)

ARL [21] is a fairness-aware method that designed to handle fairness under awareness challenges. To achieve this, ARL makes use of adversarial training to emphasize more

Table 7. Stree testing on the models for the mouth slightly open (MSO) task on CelebA dataset, by eliminating 90% FP, MN, FPMN of a subpopulation in the training/validation set. CID achieves the best results.

FP	Acc	Id Acc	10% Id Acc	δ_{id}	AUMM	AUD
CE	91.70	91.29	67.58	0.1061	0.1726	0.1349
IFW	<u>92.44</u>	<u>92.09</u>	<u>69.53</u>	<u>0.1023</u>	<u>0.1612</u>	<u>0.1300</u>
DRO	91.81	91.33	67.33	0.1059	0.1707	0.1323
IRM	91.71	91.25	67.78	0.1083	0.1729	0.1346
ARL	91.94	91.38	67.13	0.1071	0.1735	0.1311
CID	92.67	92.16	69.91	0.1000	0.1589	0.1126

MN	Acc	Id Acc	10% Id Acc	δ_{id}	AUMM	AUD
CE	92.36	91.67	68.33	0.1011	0.1662	0.1200
IFW	<u>92.67</u>	<u>92.22</u>	<u>71.17</u>	<u>0.0971</u>	<u>0.1563</u>	<u>0.1265</u>
DRO	92.54	91.89	68.37	0.1054	0.1672	<u>0.1166</u>
IRM	92.62	91.96	68.46	0.1048	0.1657	0.1192
ARL	92.34	91.86	68.59	0.1053	0.1679	0.1213
CID	92.90	92.32	71.87	0.0949	0.1560	0.1161

FPMN	Acc	Id Acc	10% Id Acc	δ_{id}	AUMM	AUD
CE	89.99	89.39	64.22	0.1238	0.2011	0.1410
IFW	89.88	89.05	65.82	0.1275	0.2033	0.1424
DRO	<u>90.02</u>	<u>89.42</u>	<u>65.93</u>	0.1211	0.1988	<u>0.1336</u>
IRM	89.99	89.35	65.41	0.1212	<u>0.1984</u>	0.1429
ARL	90.00	89.40	63.63	<u>0.1175</u>	0.1987	0.1381
CID	90.47	89.94	67.05	0.1113	0.1883	0.1295

Table 8. Gender and age Rawlsian min-max results on smiling tasks

Gender	Default	MP 90%	MN 90%	FPMN 90%
CE	0.01717	0.05047	0.07859	0.05940
IFW	0.01748	<u>0.04116</u>	<u>0.05415</u>	0.07738
DRO	0.01671	0.04901	0.07635	0.05933
IRM	<u>0.01645</u>	0.05117	0.07792	<u>0.05722</u>
ARL	0.01678	0.05366	0.07785	0.05910
CID	0.01633	0.03553	0.04893	0.04428

Age	Default	MP 90%	MN 90%	FPMN 90%
CE	0.02251	0.04167	0.06421	0.07548
IFW	0.02289	<u>0.03378</u>	<u>0.05536</u>	0.08442
DRO	0.02336	0.03838	0.06258	<u>0.07518</u>
IRM	<u>0.02251</u>	0.04001	0.06556	0.07698
ARL	0.02271	0.04136	0.06744	0.07624
CID	0.02231	0.03131	0.05288	0.06411

on the samples that make significant errors and improve improve accuracy for the protected groups. Specifically, ARL optimizes the following min-max objective:

$$\min_{\mathbf{w}} \max_{\phi} \lambda_{\phi}(\mathbf{x}_i, y_i) \ell_i(\mathbf{w}; \mathbf{x}_i, y_i) \quad (5)$$

where \mathbf{w} is the model (learner) parameters, and ϕ denotes the adversarial network, f_{ϕ} represents the output of adversarial network and $\lambda_{\phi}(\mathbf{x}_i, y_i) = 1/n + \frac{f_{\phi}(\mathbf{x}_i, y_i)}{\sum_{i=1}^n f_{\phi}(\mathbf{x}_i, y_i)}$ is the adversarial assignment of the weight vector $\lambda_{\phi} : f_{\phi} \rightarrow R$ so as to maximize the expected loss and $f_{\phi} : X \times Y \rightarrow R$ is the output of the adversary network designed to identify the regions where the model makes significant errors.

In our case, we aim to balance the positive and negative samples for each identity during the training and empha-

size more on the minorities to achieve fairness under unawareness. As the same facial features close to each other in the face recognition space, we make use of face recognition embeddings as proxy vectors of identities due to the unavailable of ground truth label information. We assign conditional inverse density robust weight p_i^{τ} to each sample defined in the neighborhood of the proxy space to balance the positive and negative samples that share the same facial features, i.e, identity.

$$\min_{\mathbf{w}} \sum_{i=1}^n \frac{p_i^{\tau}}{Z_{y_i}} \ell_i(\mathbf{w}; \mathbf{x}_i, y_i) \quad (6)$$

where n represents the size of \mathcal{D} , i.e, $n = |\mathcal{D}|$, $p_i^{\tau} = \exp(\frac{\mathbf{z}_i^{\top} \mathbf{z}_i}{\tau}) / \sum_{k=1}^{|\mathcal{D}_{y_i}|} \exp(\frac{\mathbf{z}_i^{\top} \mathbf{z}_k}{\tau})$ and τ represents the size of the neighborhood within which samples are considered to be from the same identity group. $Z_{y_i} = \sum_{j \in \mathcal{D}_{y_i}} p_j^{\tau}$ to balance class contributions.

Hence by replace $\lambda_{\phi}(\mathbf{x}_i, y_i)$ with p_i^{τ} in Equation (5), ARL share the same objective with our proposed method. Compare with p_i^{τ} , $\lambda_{\phi}(\mathbf{x}_i, y_i)$ is obtained via maximizing the objectives combined with the learner prediction losses, i.e, $\max_{\phi} \lambda_{\phi}(\mathbf{x}_i, y_i) \ell_i(\mathbf{w}; \mathbf{x}_i, y_i)$. Hence, the $\lambda_{\phi}(\mathbf{x}_i, y_i)$ is obtained based on the sample loss predictions rather than features that represent group information such as identity, which leads to poorer performance of ARL than CID in terms of identity fairness, as observed in all experiments

ARL Implementation The same as other baselines, the learner is implemented using ResNet18. For the adversarial head, we implement a linear model with sigmoid activation function where the input is the representation feature learned from learner. The learning rate of adversarial learner ϕ is tuned in $\{1e-2, 1e-3, 1e-4\}$.

8.4.2 Distributionally Robust Learning

DRO [23, 27] has been show an effective methods to improve the worst group accuracy such that the fairness can be improved. Similar to ARL, DRO

$$\min_{\mathbf{w}} \max_{\mathbf{p} \in \mathcal{U}} p_i \ell_i(\mathbf{w}; \mathbf{x}_i, y_i) \quad (7)$$

in which \mathbf{p} is defined in the uncertainty set \mathcal{U} . Hence, after getting \mathbf{p}^* by solving the inner maximization problem, the DRO reduces to a instance sample weighting method that

$$\min_{\mathbf{w}} p_i^* \ell_i(\mathbf{w}; \mathbf{x}_i, y_i) \quad (8)$$

To be more specific, when $\mathcal{U} = \{\mathbf{p} \in \Delta, \sum_{i=1}^n p_i \log np_i \leq \rho\}$ in [23, 27], where $\mathbf{p} \in \Delta : \sum_{i=1}^n p_i = 1, \sum_{i=1}^n p_i \log np_i \leq$

ρ represents the KL-divergence discrepancy constraint between \mathbf{p} and uniform sampling weights $\frac{1}{n}, 1 \in \mathbb{R}^n$. Given this uncertainty set, p_i^* has the close form of $p_i^* = \exp(\frac{\ell_i(\mathbf{w}; \mathbf{x}_i, y_i)}{\nu}) / \sum_{i=1}^n \exp(\frac{\ell_i(\mathbf{w}; \mathbf{x}_i, y_i)}{\nu})$, where ν is a Lagrange multiplier introduced by \mathcal{U} .

Therefore, we can see the instance weights p_i^* for each sample introduced by DRO is proportional to the loss scales, while our fairness robust weights p_i^τ defined on the pairwise similarity in the neighborhood face proxy embeddings of sample (\mathbf{x}_i, y_i) to balance the contribution of positive and negative classes for any arbitrary facial features that are considered belonging to the same identity.

8.4.3 Inverse Frequency Weighting (IFW)

IFW [17, 33] aims to balance the contributions of different classes by assigning class-balancing weights to each sample that is proportional to the number of samples for each class, i.e.,

$$\sum_{i=1}^n p_i \ell_i(\mathbf{w}; \mathbf{x}_i, y_i) \tag{9}$$

where $p_i \propto \frac{1}{N_{y_i}}$, where N_{y_i} represents the frequency of class y_i . As we explained in Section 4.1, our assign robust weights $p_i^\tau \rightarrow \frac{1}{|\mathcal{D}_{y_i}|}$ when $\tau \rightarrow \infty$ such that CID reduces to IFW. Hence, IFW is a special case of CID. When $\tau \in (0, \infty)$, CID considers more fine-grained rarity of local neighborhood face proxy embedding, i.e., p_i^τ balances the positive and negative samples within each local neighborhood which serves as a proxy of identity, to improve identity robustness.